



Xenobiotica

the fate of foreign compounds in biological systems



ISSN: (Print) (Online) Journal homepage: <https://www.tandfonline.com/loi/ixen20>

Metabolic Activation of Deferiprone Mediated by CYP2A6

Xiaojiao Zheng, Xu Wang, Zifang Ding, Wei Li, Ying Peng & Jiang Zheng

To cite this article: Xiaojiao Zheng, Xu Wang, Zifang Ding, Wei Li, Ying Peng & Jiang Zheng (2021): Metabolic Activation of Deferiprone Mediated by CYP2A6, *Xenobiotica*, DOI: 10.1080/00498254.2021.1931729

To link to this article: <https://doi.org/10.1080/00498254.2021.1931729>



Accepted author version posted online: 18 May 2021.



Submit your article to this journal [↗](#)



Article views: 33



View related articles [↗](#)



View Crossmark data [↗](#)

Title page

Metabolic Activation of Deferiprone Mediated by CYP2A6

Xiaojiao Zheng,¹ Xu Wang,¹ Zifang Ding,¹ Wei Li,¹ Ying Peng,^{1*} and Jiang Zheng^{1,2,3*}

¹Wuya College of Innovation, Shenyang Pharmaceutical University, Shenyang, Liaoning 110016, P. R. China

²State Key Laboratory of Functions and Applications of Medicinal Plants, Guizhou Provincial Key Laboratory of Pharmaceutics, Guizhou Medical University, Guiyang, Guizhou 550025, P. R. China

³Key Laboratory of Environmental Pollution, Monitoring and Disease Control, Ministry of Education, Guizhou Medical University, Guiyang, 550025, P. R. China

Corresponding Authors

Jiang Zheng, PhD

Wuya College of Innovation, Shenyang Pharmaceutical University, Shenyang, Liaoning 110016, P. R. China; State Key Laboratory of Functions and Applications of Medicinal Plants, Key Laboratory of Pharmaceutics of Guizhou Province, Guizhou Medical University, Guiyang, Guizhou 550025, P. R. China

E-mail: zhengneu@yahoo.com

Tel: +86-24-23984215

Fax: +86-24-23986510

Ying Peng, PhD

Wuya College of Innovation, Shenyang Pharmaceutical University, Shenyang, Liaoning 110016, P. R. China

E-mail: yingpeng1999@163.com

Tel: +86-24-23986361

Fax: +86-24-23986510

Abstract

1. Deferiprone (DFP) is a metal chelating agent generally used to treat patients with thalassemia, due to iron overload in clinical settings.
2. Studies have revealed that long-term use of DFP can induce hepatotoxicity, however, mechanisms of its toxic action remain unclear. The present studies are aimed to characterize the reactive metabolite of DFP, to define the metabolic pathway, and to determine the P450 enzymes participating in the bioactivation.
3. A demethylation metabolite (M1) was observed in rat liver microsomal incubations. Additionally, a glutathione (GSH) conjugate (M2) and an *N*-acetylcysteine (NAC) conjugate (M3) were detected in microsomal incubations fortified with DFP and GSH/NAC.
4. Biliary M2 and urinary M3 were respectively found in animals administered DFP.
5. CYP2A6 enzyme dominated the catalysis to bioactivate DFP.

Keywords: Deferiprone, Metabolic Activation, CYP2A6

Introduction

Deferiprone (DFP, 3-hydroxy-1,2-dimethyl-4(1H)-pyridone) is a metal chelating agent (Huang *et al.* 2006). In 2011, the Food and Drug Agent of the USA approved DFP for the treatment of thalassemia with poor response to existing chelation therapy and excessive iron load, due to blood transfusion (Belmont *et al.* 2017; Chuansumrit *et al.* 2016). Nowadays, it is the only metal chelating agent that can be taken orally with a strong chelating effect on iron (Kontoghiorghe *et al.* 2016). Previous studies showed that DFP can be rapidly absorbed from the upper gastrointestinal tract with T_{\max} at 45 min, rapidly metabolized and excreted by the liver and kidney (Fredenburg *et al.* 1996). However, long-term use of DFP has been shown to cause liver injury with an abnormal increase of serum alanine (Cohen *et al.* 2003; Maggio *et al.* 2002). Unfortunately, the mechanisms of DFP induced hepatotoxicity are not understood.

Metabolic activation is one of the mechanisms of drug-induced liver injury (Chi *et al.* 2016). Those drugs execute toxicities after metabolic transformation. A number of drug metabolizing enzymes have been found to participate in the bioactivation and toxicities of the drugs (Yao *et al.* 2016). Cytochrome P450 enzymes are involved in such undesired toxic effects (Lee *et al.* 2003; Venkatakrisnan *et al.* 2001). Specifically, the enzymes can catalyze the oxidation via addition of oxygen and dehydrogenation. Oxidative *N*-, *O*-, and *S*-dealkylations are the metabolic pathways catalyzed mainly by P450 enzymes. Structurally, DFP has a frame of pyridinone, along with a methyl group attached on the nitrogen. We speculated that *N*-demethylation catalyzed by P450 enzymes would take place with DFP, which may produce a quinone-like reactive metabolite. Quinones are

highly reactive electrophiles that can react with nucleophilic group occurring in biomolecules, i.e. DNA and protein (Bolton *et al.* 2000; Graham *et al.* 1978). The present study aimed to characterize metabolite(s) of DFP *in vitro* and *in vivo*, determine metabolic activation pathway(s) of DFP, and identify cytochromes P450 enzymes participating in the production of reactive metabolite(s) of DFP.

Materials and methods

Chemicals and materials. Deferiprone and maltol (purity > 98%) were obtained from Aladdin Reagent Co., Ltd. (Shanghai, China). Propranolol, glutathione (GSH), nicotinamide adenine dinucleotide phosphate (NADPH), *N*-acetyl-L-cysteine (NAC) and methoxsalen were acquired from Sigma-Aldrich Co. (St. Louis, MO). Solid phase extraction columns (Cleanert™ PAX) were obtained from Agela Technologies Co., Ltd. (Tianjin, China). Rat (Sprague-Dawley, male) liver microsomes were prepared in our laboratory according to our published procedure (Ma *et al.* 2014). Recombinant human P450 enzymes and human liver microsomes were supplied by BD Gentest (Woburn, MA). All organic solvents were purchased from Fisher Scientific (Springfield, NJ). All of the reagents and solvents were of analytical or HPLC grade.

Microsomal incubations. DFP was dissolved in PBS buffer to prepare the stock solution. A microsomal incubations mixture was prepared by mixing DFP (100 μ M) or M1 (100 μ M) with rat or human hepatic microsomes (1.0 mg protein/mL) supplemented with GSH or NAC (20 mM) in PBS buffer (pH 7.4, final volume of 250 μ L). The concentration was selected according to a study where the fasting serum concentration of DFP can reach

126 $\mu\text{mol/L}$ at a dose of 25 mg/kg (Bellanti *et al.* 2014). Reactions were launched by adding NADPH (1.0 mM), and the incubations were carried out at 37 °C for 45 min. The reactions were terminated by the same volume of ice-cold acetonitrile, vortexed for 3 min, and centrifuged at 19,000 *g* for 10 min. The resultant supernatants (5 μL) were analyzed by an LC-MS/MS system. Control incubations lacked NADPH, NAC or GSH. All incubation experiments were carried out in duplicate.

Chemical synthesis of M1. Synthetic M1 was prepared (Scheme 1) as described by Dong and co-workers (Dong *et al.* 2018). Briefly, maltol (0.756 g, 6 mmol) was mixed with aqueous ammonia (5 mL, 20%) in a round bottom flask. The resultant mixture was slowly stirred at 45 °C for 2 h and then mixed dropwise with carbonic acid (1.73 g, 18 mmol) dissolved in 5 mL water within 5 h with stirring and refluxed for 5 h. Thin layer chromatography was used to monitor the reaction. The resulting mixture was cooled to 0 °C, filtered, rinsed with water, and dried to offer crude products. The crude product was submitted to a semipreparative HPLC system for purification, followed by characterization by NMR and mass spectrometry.

Synthesis of M2 and M3. A mixture of M1 (0.625 g, 5 mmol) and Ag_2O (3 g, 6 mmol) was stirred in methanol (40 mL) at 45 °C for 2 h (Li *et al.* 1999). The resulting solid was removed by filtration and the filtrates were condensed by rotary evaporation. The crude product was recrystallized from ether to give bright yellow crystals. GSH (1.842 g, 6 mmol) or NAC (0.978 g, 6 mmol) was dissolved in CH_2Cl_2 (75 mL) containing synthetic M1 (0.492 g, 4 mmol). The reaction mixture was stirred for 8 h at room

temperature and condensed by rotary evaporation and submitted to the semipreparative HPLC system for purification. The purified product was characterized by NMR and mass spectrometry.

Animal experiments. Sprague-Dawley rats (male, 200 ± 10 g) were obtained from the Animal Center of Shenyang Pharmaceutical University. All animal raising and experiments were conducted by following the Animal Experimental Regulations of Ethics Review Committee of Shenyang Pharmaceutical University (license number: SYPU-IACUC-C2019-9-2-204). Animals were kept in a controlled environment with a 12 h cycle of light and darkness and fed with water and food freely. Rats were randomly divided into two groups (three for each). Animals were fasted for 12 h before the experiment and anesthetized by administering (*i.p.*) urethane (20%) at a dose of 1.35 g/kg. We used at least three different batches of rats. Bile ducts were cannulated, and blank bile was harvested. Subsequently the rats were administered (*i.p.*) DFP (140 mg/kg) dissolved in saline, according to early literature (Gong *et al.* 2010), and 0-4 h bile samples were harvested. The other three animals were given the same dose of DFP and placed in metabolism cages, and 0-24 h urine samples were harvested individually. Blank urine samples were collected from these animals before DFP administration.

Sample preparation. The resulting urine or bile samples (300 μ L) were mixed with acetonitrile (900 μ L), vortexed, and centrifuged. The supernatants were condensed by blowing with nitrogen flow and cleaned by solid phase extraction column. Briefly, SPE columns were washed with methanol (10 mL) and then glacial acetic acid-water solution

(10 mL, pH=3.5). The samples were acidified with acetic acid to pH 3 and loaded onto the column. The resulting column was eluted with a gradient of methanol-water (pH=3.5) solution at concentrations of 0, 20, 40, 60, and 80% (10 mL for each). The target eluates were pooled and concentrated by blowing with N₂ flow. The resulting concentrates were dissolved in 100 μ L of 5% acetonitrile in water, followed by 10 min centrifugation at 19,000 g. The resultant supernatants (5 μ L) were subjected to LC-MS/MS for analysis.

Recombinant human P450 enzyme incubations. To identify the specific P450 enzymes participating in the production of reactive metabolites of DFP, nine human recombinant P450s, i.e. CYPs3A5, 3A4, 2E1, 2D6, 2C19, 2C9, 2B6, 2A6, and 1A2, were tested. Individual human recombinant P450 enzymes (100 nmol enzyme with a total volume of 100 μ L in each incubation) were incubated with DFP and NAC under similar condition for microsomal incubations. The resulting reactions were quenched by ice-cold acetonitrile (100 μ L) spiked with propranolol (5.0 ng/mL) as the internal standard. Produced metabolites of DFP were assessed using an LC-MS/MS system. Each incubation was carried out in triplicate.

Microsomal inhibition study. The incubation system contained DFP (100 μ M), MgCl₂ (3.2 mM), methoxsalen (10 μ M), NAC (20 mM), PBS (100 mM, pH 7.4), rat or human hepatic microsomes (1.0 mg protein/mL), and NADPH (1.0 mM). The control reaction mixture lacked methoxsalen. The resulting reactions were quenched by the same volume of ice-cold acetonitrile spiked with propranolol (5.0 ng/mL) as the internal standard.

Cytotoxicity Evaluation. MTT assay was performed in cultured rat primary hepatocytes to evaluate the cytotoxicity of DFP. Cells were isolated according to a modified two-step collagenase perfusion method (Shen *et al.* 2012). After dissociating from anesthetized adult rats, hepatocytes were seeded in 96-wells plates at a density of 1.8×10^4 cells/well and incubated for nearly 8 h for recovering and adhering. The resulting cells were treated with DFP at concentrations of 0, 5, 10, 25, 50, 100 and 200 μM . In control groups, cells received PBS buffer. The resultant cells were incubated at 37 °C in a humidified incubator with 5% CO_2 for 12 h, followed by addition of 10 μL of MTT solution (5.0 mg/mL). The media were discarded 4 h later, and DMSO (100 μL) was added to dissolve the formazan crystals. Cell viability was determined by measuring the absorbance at 562 nm. The cytotoxicity tests were carried out in triplicate.

LC-MS/MS methods. Metabolite analysis and assessment, along with internal standard quantification, were conducted on an AB SCIEX Instruments 4000 Q-Trap (Applied Biosystems, Foster City, CA) equipped with an Agilent 1260 infinity HPLC system (Agilent Technologies, Biblengen, Germany). Analytes were separated on an Accuore C_{18} column (4.6 \times 250 mm, 5 μm , Dikma Technological). The column was eluted with a mobile system composed of acetonitrile with 0.1 % formic acid (A) and 0.1 % formic acid in water (B), using a gradient elution program as follows: 5 % A at 0-2 min; 5-30 % A at 2-4 min; 30-90 % A at 4-10 min; 90 % A at 10-11 min; 90-10 % A at 11-12 min; 5 % A at 12-14 min. The flow rate was set at 0.5 mL/min, and the column temperature was kept at 25 °C. Mass spectrometric parameters were set as follows: ion spray voltage: 5500 V; curtain gas 1: 20 psi; curtain gas 2: 20 psi; temperature of the turbo

ion spray: 600 °C; entrance potential: 10 V; and cell exit potential: 3 V. Optimal response for the analysis in positive ion mode was achieved by multiple-reaction monitoring (MRM) scanning. Characteristic ion pairs (declustering potential (DP), collision energy (CE)) were m/z 140→96 (95, 35) for DFP, m/z 126→108 (85, 35) for M1, m/z 431→158 (100, 40) for DFP-GSH conjugate, m/z 287→158 (100, 40) for DFP-NAC conjugate, and m/z 260→116 (70, 30) for propranolol separately. Information-dependent acquisition (IDA) was used to initiate enhanced product ion (EPI) scanning by analyzing MRM signals. EPI scanning was run in positive ion mode for product ion ranging from m/z 100 to 900. IDA was set to select ions more than 2000 cps with the exclusion of former target ions after three occurrences for 10 s and collision energy was set at 35 eV with a spread of 15 eV. Additionally, an AB SCIEX Instruments 5500 triple quadrupole mass spectrometry (Applied Biosystems, Foster City, CA) equipped with an Agilent 1260 infinity LC system (Agilent Technologies, Biblengen, Germany) was also employed to analyze DFP and its metabolites with the same parameters as those mentioned above. The AB SCIEX Instruments 4000 triple quadrupole mass spectrometry equipped with Q-trap was used to acquire tandem mass spectra of analytes. The AB SCIEX Instruments 5500 triple quadrupole mass spectrometry was employed for quantitative analysis, due to higher sensitivity. All data obtained were processed by AB SCIEX Analyst 1.6.3 software (Applied Biosystems).

In addition, a hybrid quadrupole-time-of-flight mass spectrometry (Bruker micro Q-TOF, Germany) with an ESI source coupled to an Agilent 1200 Series LC system was used for the characterization of synthetic products in positive ion mode. Mass

spectrometry parameters were optimized as below: ionization temperature was maintained at 180 °C; nebulizer gas pressure, 1.2 bar; dry gas flow rate, 8.0 L/min; capillary voltage, -4500 V; end plate offset, 2500 V. Mass spectra were acquired at 2 s per spectrum from m/z 50 to 1500. Analytes were separated using the same LC protocol described above. The resulting data were processed by use of Bruker Daltonics Data Analysis 3.4 software.

Statistical analysis. All obtaining data were processed using GraphPad Prism 8 (GraphPad Software, San Diego, CA, USA) and expressed as means \pm SD. Unpaired Student's *t*-test was applied for statistical analysis. The values of $p < 0.05$ were deemed to have significant differences.

Accepted Manuscript

Results

Oxidative demethylation of DFP in microsomal incubations. In microsomal incubations supplemented with DFP, a demethylation metabolite (M1) with retention time of 6.38 min was detected by monitoring ion pair m/z 126/108. Product ion m/z 108 of M1 was acquired by MRM-IDA-EPI scanning and generated by the breaking of the C-O bond (Figure 1C). No such metabolite was detected in microsomal incubations lacking NADPH (Figure 1A). M1 was synthesized by amination of maltol in aqueous NH_3 (Scheme 1) and then characterized by NMR and mass spectrometry. $^1\text{H-NMR}$ (400 MHz, $\text{DMSO-}d_6$): δ 11.39 (s, 1H), 7.40 (d, $J = 6.9$ Hz, 1H), 6.09 (d, $J = 6.9$ Hz, 1H), 2.17 (s, 3H). As expected, synthetic M1 displayed similar retention time (6.35 min) and mass spectrum as that detected in microsomal incubations (Figure 1D and E).

Formation of quinone metabolite derived from DFP in microsomal incubations. Microsomal incubations were conducted in which GSH was included as the trapping agent. A GSH conjugate (M2) at retention time of 10.37 min was detected in GSH-supplemented rat microsomal incubations. Formation of M2 was monitored by acquiring precursor/product ion pair at m/z 431/158 in positive ion mode (Figure 2B). The tandem mass spectrum of M2 demonstrated product ions at m/z 158, 302, 355 and 199. The fragment ion at m/z 158, the major fragment ion, was generated by the breaking of the C-S bond of the conjugate. Fragment ion m/z 302 was formed by the neutral loss (NL) of the γ -glutamyl moiety (-129 Da) from m/z 431. Formation of the product ion at m/z 355 resulted from cleavage of the glycine group (-75 Da). The characteristic ion at m/z 199 derived from m/z 302 was formed by the loss of the *N*-formylglycinyl group (-103 Da).

Control incubation lacking NADPH failed to produce such conjugate (Figure 2A). Similar *in vitro* incubations were carried out in human liver microsomes. As expected, we detected a GSH conjugate with similar retention time and mass spectral property (Figure S1). Biomimetic synthesis of M2 was carried out by oxidation of synthetic M1 using Ag₂O and then conjugating with GSH. The obtained product demonstrated similar chromatographic property and mass spectrum (Figure 2D and E) as that detected in GSH-fortified rat microsomal incubations of DFP.

Similar microsomal incubations were conducted which contained NAC in place of GSH as the tapping agent. By monitoring ion pair m/z 287/158, an NAC conjugate (M3) with the retention time of 10.41 min was detected (Figure 3B) in the incubations. The tandem mass spectrum obtained from MRM-IDA-EPI scanning showed product ions at m/z 158, 130 and 84. The characteristic product ion at m/z 158 was generated by the breaking of the C-S bond in NAC moiety (-129 Da) and fragment ion m/z 130 due to S-C cleavage at NAC side. In addition, product ion m/z 84 was the most characteristic fragment ion for the parent moiety (Figure 3C). As expected, no such NAC conjugate was detected in microsomal incubations lacking NADPH (Figure 3A). Meanwhile, we found the same NAC conjugate in human liver microsomal incubations (Figure S2). M3 was synthesized through oxidation of M1 by Ag₂O and then reaction with NAC. The resultant synthetic product was characterized by NMR and mass spectrometry. The protonated molecular ion of the product was m/z 287.0691 (HPLC-Q-TOF). According to the predicted formula, the error between the accurate mass observed in the high-resolution MS system and the corresponding theoretical mass was less than 5 ppm (Table 1). ¹H-NMR

(600 MHz, Deuterium Oxide): δ 7.00 (s, 1H), 4.49 (dd, $J = 7.4, 4.1$ Hz, 1H), 3.60 (dd, $J = 14.6, 4.2$ Hz, 1H), 3.36 (dd, $J = 14.6, 7.5$ Hz, 1H), 2.44 (s, 3H), 1.90 (s, 3H) (Figure S3B and 4B). The synthetic M3 displayed similar chromatographic behavior and mass spectral property as M3 observed in NAC-fortified microsomal incubations of DFP.

Biliary and urinary phase II metabolites of DFP. M2 was observed in bile of rats given DFP by acquiring ion pair m/z 431/158, while we failed to observe biliary M2 in rats given vehicle (Figure 5A and 5B). M2 was found to show similar retention time and mass spectral behavior as synthetic M2. Urinary M3 was found in rats administered DFP. The detected metabolite displayed the same chromatographic identity and similar mass spectral property as that of synthetic M3 (Figure 5E and 5F). As expected, M3 was not detected in the urine of animals given vehicle.

Requirement of N-demethylation for metabolic activation of DFP. Microsomal incubations of synthetic M1 supplemented with GSH or NAC were performed to define the metabolic activation pathway. Both GSH and NAC conjugates were detected in the GSH- or NAC-supplemented microsomal incubations (Figure S4). The two conjugates demonstrated similar chromatographic and mass spectral identities as biliary M2 and urinary M3 observed in animals treated with DFP. As expected, M2 and M3 were not detected in NADPH-free microsomal incubations.

P450 enzymes responsible for bioactivation of DFP. Individual CYPs3A5, 3A4, 2E1, 2D6, 2C19, 2C9, 2B6, 2A6, and 1A2 were incubated with DFP supplemented with NADPH and NAC. The resultant mixtures were submitted to LC-MS/MS analysis, and

NAC conjugate was determined to monitor the formation of DFP-derived the reactive metabolite. CYP2A6 was found to be the primary enzyme participating in the generation of M3 (Figure 6).

Effect of methoxsalen on formation of M3. Methoxsalen as a general inhibitor of CYP2A6 (Sellers *et al.* 2000) was used to verify the role of CYP2A6 in the formation of M3 *in vitro*. The contents of M3 were assessed by LC-MS/MS. M3 detected in a solvent-treated group was normalized as 100%. As depicted in Figure 7, the presence of methoxsalen resulted in 78% inhibition of the formation of M3 in human microsomal incubations, and 64% inhibition in rat microsomal incubations.

Effect of DFP on cell viability. The cytotoxicity was evaluated in rat primary hepatocytes. No significant cell death was observed after 12 h cell exposure at up to concentration of 200 μ M (Figure S5).

Discussion

DFP is commonly used as an iron depleter in clinic practice, due to its low price. Recently, many cases of liver damage caused by DFP have been reported (Xie *et al.* 2016; Ceci *et al.* 2015), but the mechanisms of the toxicity have not been elucidated. A study demonstrated that DFP is mainly excreted from urine as parent and glucuronide forms (Fradette *et al.* 2016), and limited DFP is metabolized through glucuronidation (Gong *et al.* 2010). Here, we proposed a metabolic activation pathway of DFP mediated by P450 for the better understanding of the hepatotoxicity of DFP.

Firstly, we examined mass spectrometric identity of DFP, which would assist the identification of metabolites. DFP displayed the molecular ion at m/z 140 and fragments of m/z 122, 108, and 96 (Figure S6) in positive ion mode.

Metabolism study was carried out in rat liver microsomal incubations supplemented with DFP. M1 was not detected in control group which lacked NADPH (Figure 1A). This suggests that NADPH participated in the generation of the oxidative metabolite. M1 displayed its molecular ion at m/z 126 with 14 Da less than that of DFP, suggesting that M1 was a demethylation metabolite after metabolic loss of $-CH_3$ of DFP. We also performed similar incubations using human liver microsomes, but failed to detect M1, possibly due to the detection limitation, while M1 was detected in CYP2A6 incubations (Figure S7). This suggests that the metabolic demethylation was taking place in human microsomes. Then we conducted similar incubations fortified with M1 in place of DFP and then detected M3 (Figure S8), indicating DFP is activated via the same pathway in humans as that in rats.

GSH and NAC were used to capture reactive intermediates resulting from metabolic activation of DFP (Chen and Cai 1999; Du *et al.* 2017; Zhang *et al.* 2017). GSH conjugate M2 and NAC conjugate M3 were detected in rat and human liver microsomal incubations containing DFP and GSH/NAC (Figures 2B and 3B; S1 and S2). This clearly indicates that an electrophilic intermediate was formed in DFP-supplemented rat liver microsomes. Then we incubated synthetic M1 with rat liver microsomes fortified with GSH or NAC and detected M2 and M3 in the corresponding incubation systems. This suggests that M1 was a metabolite responsible for the formation of the two conjugates.

Chemical synthesis was conducted for metabolite identification. The synthetic M1 characterized by NMR (Figures S3A and 4B) revealed the same retention time and fragments as M1 detected in microsomal incubations (Figures 1D and E). The resultant conjugates showed similar retention time and fragments (Figures 2D, 2E, 3D and 3E) as M2 and M3 detected in microsomal incubations as well as in bile and urine samples obtained from rats given DFP. Unfortunately, we did not obtain enough amount of M2 for NMR analysis.

Metabolic oxidation of M1 could also produce a *p*-quinone methide intermediate which can react with NAC and form a NAC conjugate with the same molecular weight as that of M3. If the quinone methide were generated, we would have obtained the NAC conjugate resulting from 1,4-addition at benzylic position. The NMR spectrum of M3 (Figure 4) excludes the possibility for the formation of such quinone methide intermediate, since NAC was found to attach on the aromatic ring of M3.

Recombinant human P450 enzyme incubation study showed that CYP2A6 played the major role in the metabolic activation of DFP (Figure 6). However, we cannot exclude the contribution of other P450 enzyme to the bioactivation, particularly multiple P450 enzymes are involved in the metabolic activation of DFP. Although some drugs are reportedly metabolized by human CYP2A6 but not necessarily by rat CYP2A1/2 (Miksys *et al.* 2000; Messina *et al.* 1997), rat CYP2A1/2 are known to share about 60% homology in amino acid sequence with human CYP2A6 (Martignoni *et al.* 2006). Our microsomal inhibition study showed that the presence of methoxsalen inhibited the formation of M3 in both human and rat microsomal incubations (Figure 7). Despite this, more work is in need to ensure rat CYP2A1/2 and human CYP2A6 share the similarity in catalysis of the metabolic activation of DFP.

GSH conjugates are often considered to be biomarkers for exposure to electrophiles (Chen and Cai 1999). Two-step metabolic degradation of GSH conjugates mediated by γ -glutamyltranspeptidase and dipeptidases produces the corresponding cysteine conjugates. Sequential *N*-acetylation of cysteine conjugates offers NAC conjugates (mercapturic acids) (Clapp and Young 1970). As expected, both biliary DFP-derived GSH conjugate and urinary DFP-derived NAC conjugate were detected in DFP-administered rats (Figures 5B and E). Besides, we analyzed plasma in rats, but neither M1 nor DFP-derived GSH/NAC conjugates were detected in rats given DFP.

The observed GSH/NAC conjugates suggest the formation of the *o*-quinone metabolite of DFP, and this electrophilic species may react with nucleophilic group of liver proteins. These GSH/NAC conjugates were detected in both rat and human

microsomal incubations fortified GSH or NAC. It is our speculation that the metabolic action of DFP would take place in patients administered DFP. Besides, the elimination of DFP in liver is slow relative to that of other tissues. The accumulated DFP in liver (Gong *et al.* 2010) could be responsible for the reported DFP-associated liver injury.

Given together, DFP was metabolized to M1 by oxidative *N*-demethylation (Scheme 2). M1, a hydroquinone derivative, was sequentially oxidized to *o*-quinone intermediate M4 which reacted with GSH to produce M2 (a GSH conjugate). M2 was biotransformed to M3 (a NAC conjugate).

In summary, the present work appeared to report, for the first time, the metabolic activation of DFP. The bioactivation was achieved by *N*-demethylation and then oxidation to produce *o*-quinone intermediate. CYP2A6 was involved in the metabolic activation of DFP. This finding lays the groundwork for better understanding the mechanisms of the reported DFP-induced liver injury.

Funding Information

This work was supported in part by the National Natural Science Foundation of China [Grants 81773813 and U1812403].

Conflict of interest

The authors declare no competing financial interest.

Abbreviation

NADPH, β -nicotinamide adenine dinucleotide 2'-phosphate reduced tetra sodium salt; RLMs, rat liver microsomes; HLMs, human liver microsomes; PBS, phosphate-buffered saline; DMSO, dimethyl sulfoxide; NMR, nuclear magnetic resonance; ESI, electrospray ionization; MRM, multiple-reaction monitoring; LC-MS/MS, liquid chromatography-tandem mass spectrometry; Q-TOF, quadrupole-time-of-flight; SPE, solid phase extraction.

Reference

- Bellanti F, Danhof M, Della Pasqua O. (2014). Population pharmacokinetics of deferiprone in healthy subjects. *British journal of clinical pharmacology*, 78(6), 1397–1406.
- Belmont A, Kwiatkowski JL. (2017). Deferiprone for the treatment of transfusional iron overload in thalassemia. *Expert review of hematology*, 10, 493-503.
- Bolton JL, Trush MA, Penning TM, Dryhurst G, Monks TJ. (2000). Role of quinones in toxicology. *Chemical research in toxicology*, 13, 135-60.
- Ceci A, Baiardi P, Felisi M, MD Cappellini, Tricta F. (2015). The safety and effectiveness of deferiprone in a large-scale, 3-year study in italian patients. *British Journal of Haematology*, 118(1), 330-336.
- Chen YF, Cai H. (1999). Investigation of liver damage associated with traditional Chinese medicines. *Adverse Drug Reactions Journal*, 1, 27-32.
- Chi M, Peng Y, Zheng J. (2016). Characterization of glutathione conjugates derived from reactive metabolites of bakuchiol. *Chemico-biological interactions*, 244, 178-86.
- Chuansumrit A, Songdej D, Sirachainan N, Wongwerawattanakoon P, Kadegasem P, Sasanakul W. (2016). Safety profile of a liquid formulation of deferiprone in young children with transfusion-induced iron overload: a 1-year experience. *Paediatrics and international child health*, 36, 209-13.
- Clapp JJ, Young L. (1970). Formation of mercapturic acids in rats after the administration of aralkyl esters. *The Biochemical journal*, 118, 765-71.
- Cohen AR, Galanello R, Piga A, De Sanctis V, Tricta F. (2003). Safety and effectiveness of long-term therapy with the oral iron chelator deferiprone. *Blood*, 102, 1583-7.
- Dong LJ, Sun JG, Liu J. (2018). A preparation method of pantoprazole intermediate 2-chloromethyl 3,4-dimethoxypyridine hydrochloride. *CN 105111187 A*.
- Du Q, Wang Z, Yun N, Huang Y, Xu Q, Wang BH. (2017). Literature Analysis of 185 Cases of ADR Induced by Xianling Gubao Capsule. *China Pharmacy*, 28, 3785-3787.
- Fradette C, Pichette V, Sicard É, Stilman A, Jayashankar S, Tsang Y C, Spino M, Tricta F. (2016). Effects of renal impairment on the pharmacokinetics of orally administered

- deferiprone. *British journal of clinical pharmacology*, 82(4), 994-1001.
- Fredenburg AM, Sethi RK, Allen DD, Yokel RA. (1996). The pharmacokinetics and blood-brain barrier permeation of the chelators 1,2 dimethyl-, 1,2 diethyl-, and 1-[ethan-1'ol]-2-methyl-3-hydroxypyridin-4-one in the rat. *Toxicology*, 108, 191-9.
- Gong QQ, Liu P, Zhang YN, Xu HL, Jia XJ. (2010). Pharmacokinetics and tissue distribution of deferiprone in rats. *Chinese Journal of Pharmacology and Toxicology*, 24, 59-63.
- Graham DG, Tiffany SM, Bell WR Jr, Gutknecht WF. (1978). Autoxidation versus covalent binding of quinones as the mechanism of toxicity of dopamine, 6-hydroxydopamine, and related compounds toward C1300 neuroblastoma cells in vitro. *Molecular pharmacology*, 14, 644-53.
- Huang XP, Spino M, Thiessen JJ. (2006). Transport kinetics of iron chelators and their chelates in Caco-2 cells. *Pharmaceutical research*, 23, 280-90.
- Knutsen HK, Alexander J, Barregård L, Bignami M, Brüschweiler B, Ceccatelli S, Cottrill B, Dinovi M, Edler L, Grasl-Kraupp B and others. (2017). Risks for public health related to the presence of furan and methylfurans in food. *European Food Safety Authority*, 15.
- Kontoghiorghes CN, Kontoghiorghes GJ. (2016). New developments and controversies in iron metabolism and iron chelation therapy. *World journal of methodology*, 6, 1-19.
- Lee S, Kim JM, Chung CS, Cho KJ, Kim JH. (2003). Polymorphism in CYP2C9 as a non-critical factor of warfarin dosage adjustment in Korean patients. *Archives of pharmacal research*, 26, 967-72.
- Li MS, Ma L, Zhang XC. (1999). Synthesis of substituted 1,2-benzoquinones and substituted 3-hydroxy-4 (1H) -pyridinones: Application of oxidation-Michael addition in organic synthesis. *Chinese Journal of Chemistry*, 17, 377-383.
- Maggio A, D'Amico G, Morabito A, Capra M, Ciaccio C, Cianciulli P, Di Gregorio F, Garozzo G, Malizia R, Magnano C and others. (2002). Deferiprone versus deferoxamine in patients with thalassemia major: a randomized clinical trial. *Blood cells, molecules & diseases*, 28, 196-208.
- Ma JY, Zhou X, Fu J, Hu T, Or PM, Feng R, He CY, Chen WJ, Zhang X, Chen Y and

- others. (2014). Metabolite profiling analysis of FR429, an ellagitannin purified from *Polygonum capitatum*, in rat and human liver microsomes, cytosol and rat primary hepatocytes in vitro. *Chemico-biological interactions*, 220, 33-40.
- Martignoni M, Groothuis G M, de Kanter R. (2006). Species differences between mouse, rat, dog, monkey and human CYP-mediated drug metabolism, inhibition and induction. *Expert opinion on drug metabolism & toxicology*, 2(6), 875-894.
- Messina E S, Tyndale R F, Sellers E M. (1997). A major role for cyp2a6 in nicotine c-oxidation by human liver microsomes. *Journal of Pharmacology and Experimental Therapeutics*, 282(3), 1608-1614.
- Miksys S, Hoffmann E, Tyndale R F. (2000). Regional and cellular induction of nicotine-metabolizing cyp2b1 in rat brain by chronic nicotine treatment. *Biochemical Pharmacology*, 59(12), 1501-1511.
- Rodrigues AD. (1999). Integrated cytochrome P450 reaction phenotyping: attempting to bridge the gap between cDNA-expressed cytochromes P450 and native human liver microsomes. *Biochemical pharmacology*, 57, 465-80.
- Sellers E M, Kaplan H L, Tyndale R F. (2000). Inhibition of cytochrome P450 2A6 increases nicotine's oral bioavailability and decreases smoking. *Clinical pharmacology and therapeutics*, 68(1), 35-43.
- Shen L, Hillebrand A, Wang D Q, Liu M. (2012). Isolation and primary culture of rat hepatic cells. *Journal of visualized experiments : JoVE*, (64), 3917.
- Venkatakrisnan K, Von Moltke LL, Greenblatt DJ. (2001). Human drug metabolism and the cytochromes P450: application and relevance of in vitro models. *Journal of clinical pharmacology*, 41, 1149-79.
- Xie YY, Lu Z, Kong XL, Zhou T, Bansal S, Hider R. (2016). Systematic comparison of the mono-, dimethyl- and trimethyl 3-hydroxy-4(1H)-pyridones - Attempted optimization of the orally active iron chelator, deferiprone. *European journal of medicinal chemistry*, 115, 132-40.
- Yao H, Peng Y, Zheng J. (2016). Identification of glutathione and related cysteine conjugates derived from reactive metabolites of methyleugenol in rats. *Chemico-Biological Interactions*, 253, 143-152.

Table legend

Table 1. Data of DFP-NAC Conjugate (M3) Obtained from HPLC-Q-TOF MS Analysis.

Figure legends

Figure 1. Characterization of oxidative M1. Extracted ion (m/z 126/108) chromatograms collected from LC-MS/MS analysis of rat liver microsomal incubations containing DFP in the absence (A) or presence (B) of NADPH; C: Tandem mass spectrum of M1 formed in rat microsomal incubations; D: Extracted ion (m/z 126/108) chromatogram collected from LC/MS-MS analysis of synthetic M1; E: Tandem mass spectrum of synthetic M1.

Figure 2. Characterization of M2. Extracted ion (m/z 431/158) chromatograms collected from LC-MS/MS analysis of rat liver microsomal incubations containing DFP and GSH in the absence (A) or presence (B) of NADPH; C: Tandem mass spectrum of M2 generated in rat microsomal incubations; D: Extracted ion (m/z 431/158) chromatogram collected from LC/MS-MS analysis of synthetic M2; E: Tandem mass spectrum of synthetic M2.

Figure 3. Characterization of M3. Extracted ion (m/z 287/158) chromatograms acquired from LC-MS/MS analysis of rat liver microsomal incubations containing DFP and NAC in the absence (A) or presence (B) of NADPH; C: Tandem mass spectrum of M3 generated in rat microsomal incubations; D: Extracted ion (m/z 287/158) chromatogram collected from LC/MS-MS analysis of synthetic M3; E: Tandem mass spectrum of synthetic M3.

Figure 4. Structures (A) and $^1\text{H-NMR}$ profiles (B) of M1 and M3.

Figure 5. Characterization of biliary M2 and urinary M3. Chromatograms of extracted ion (m/z 431/158 for M2) acquired from LC-MS/MS analysis of bile harvested from rats before (A) and after (B) administration of DFP; C: Tandem mass spectrum of biliary M2 in rats treated with DFP; Chromatograms of extracted ion (m/z 287/158 for M3) obtained from LC-MS/MS analysis of urine of rats before (D) and after (E) treatment with DFP; F: Tandem mass spectrum of urinary M3 in rats administered DFP.

Figure 6. Role of individual human recombinant P450 enzymes in the metabolic activation of DFP. The catalytic capabilities of the enzymes were evaluated by monitoring the formation of M3 after normalization according to the relative contents of the corresponding P450 enzymes in human liver microsomes. The most abundant metabolite M3 was deemed as 100%. Data represent the mean \pm SD (n = 3).

Figure 7. Inhibitory effect of methoxsalen (10 μ M) on the formation of metabolite M3 in human (A) and rat (B) liver microsomal incubations containing NAC and NADPH. The generation of M3 in control groups without methoxsalen was deemed as 100%. Data represent the mean \pm SD (n = 3). * p < 0.05; ** p < 0.01 versus their respective incubations without methoxsalen.

Scheme legends

Scheme 1. Synthetic route of M1.

Scheme 2. Proposed metabolic pathways of DFP mediated by CYP2A6.

Table 1. Data of DFP-NAC Conjugate (M3) Obtained from HPLC-Q-TOF MS Analysis.

Compound	Formula	[M+H] ⁺		Error		
		Calculated	Detected	ppm	mDa	mSigma
M3	C ₁₁ H ₁₅ N ₂ O ₅ S	287.0696	287.0691	1.7	0.50	7.70

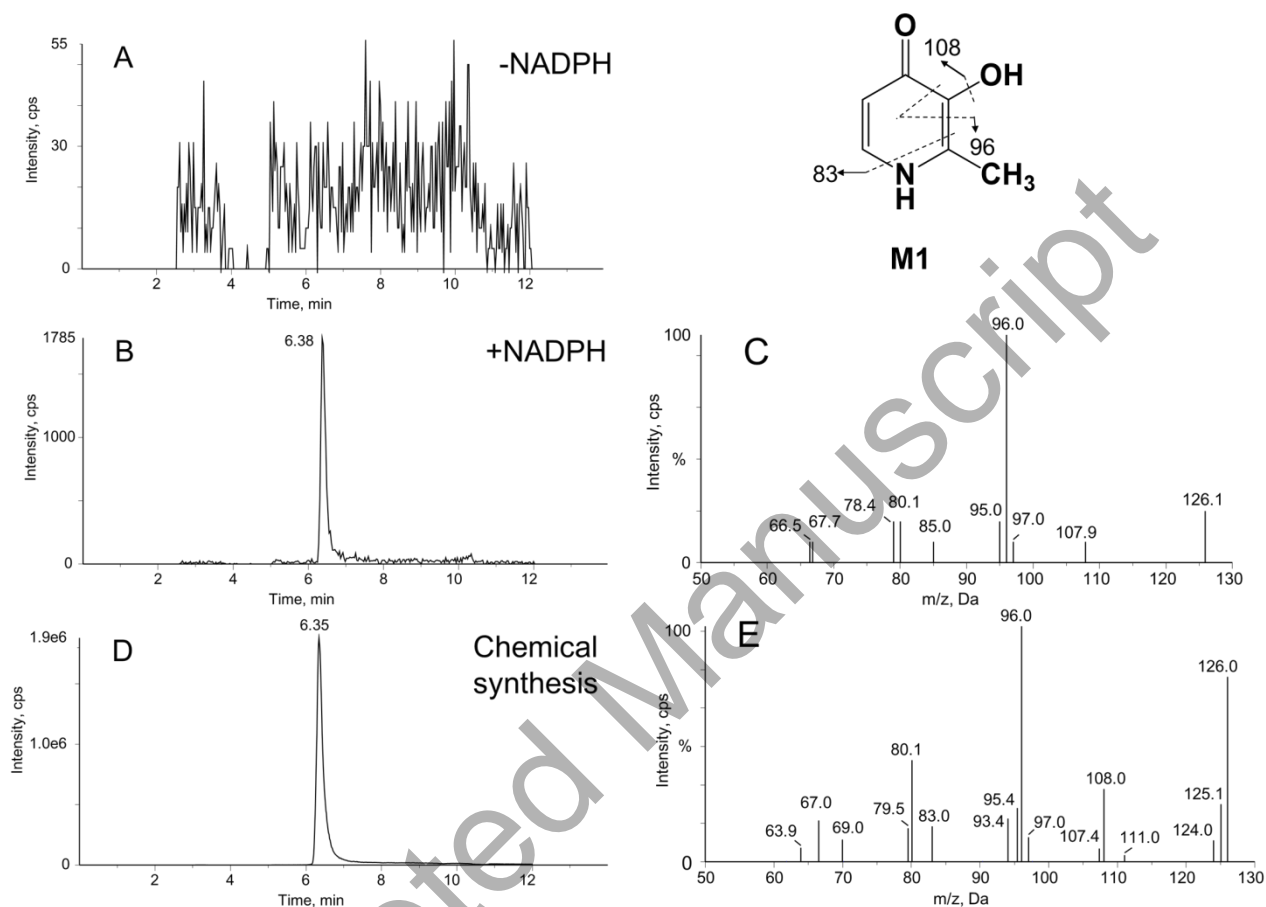


Figure 1. Characterization of oxidative M1. Extracted ion (m/z 126/108) chromatograms collected from LC-MS/MS analysis of rat liver microsomal incubations containing DFP in the absence (A) or presence (B) of NADPH; C: Tandem mass spectrum of M1 formed in rat microsomal incubations; D: Extracted ion (m/z 126/108) chromatogram collected from LC/MS-MS analysis of synthetic M1; E: Tandem mass spectrum of synthetic M1.

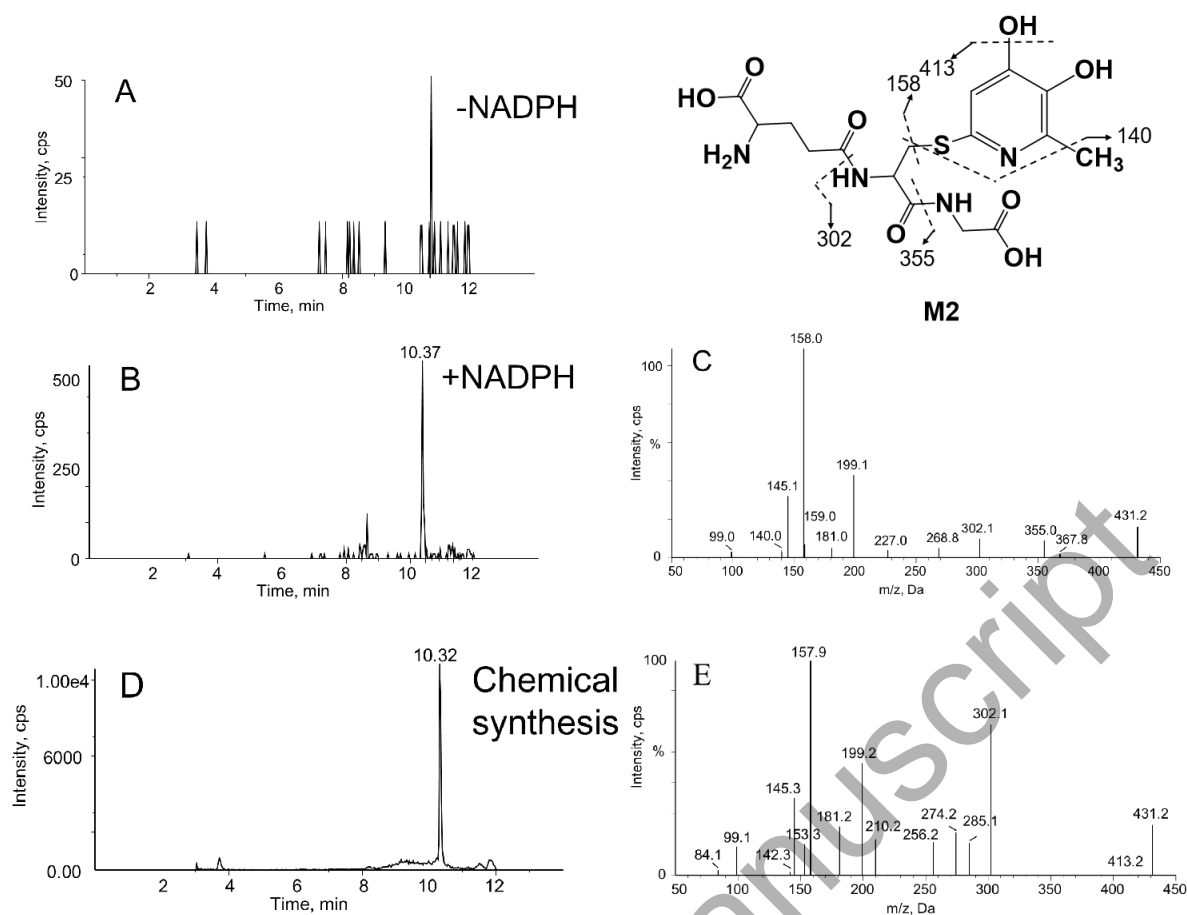


Figure 2. Characterization of M2. Extracted ion (m/z 431/158) chromatograms collected from LC-MS/MS analysis of rat liver microsomal incubations containing DFP and GSH in the absence (A) or presence (B) of NADPH; C: Tandem mass spectrum of M2 generated in rat microsomal incubations; D: Extracted ion (m/z 431/158) chromatogram collected from LC/MS-MS analysis of synthetic M2; E: Tandem mass spectrum of synthetic M2.

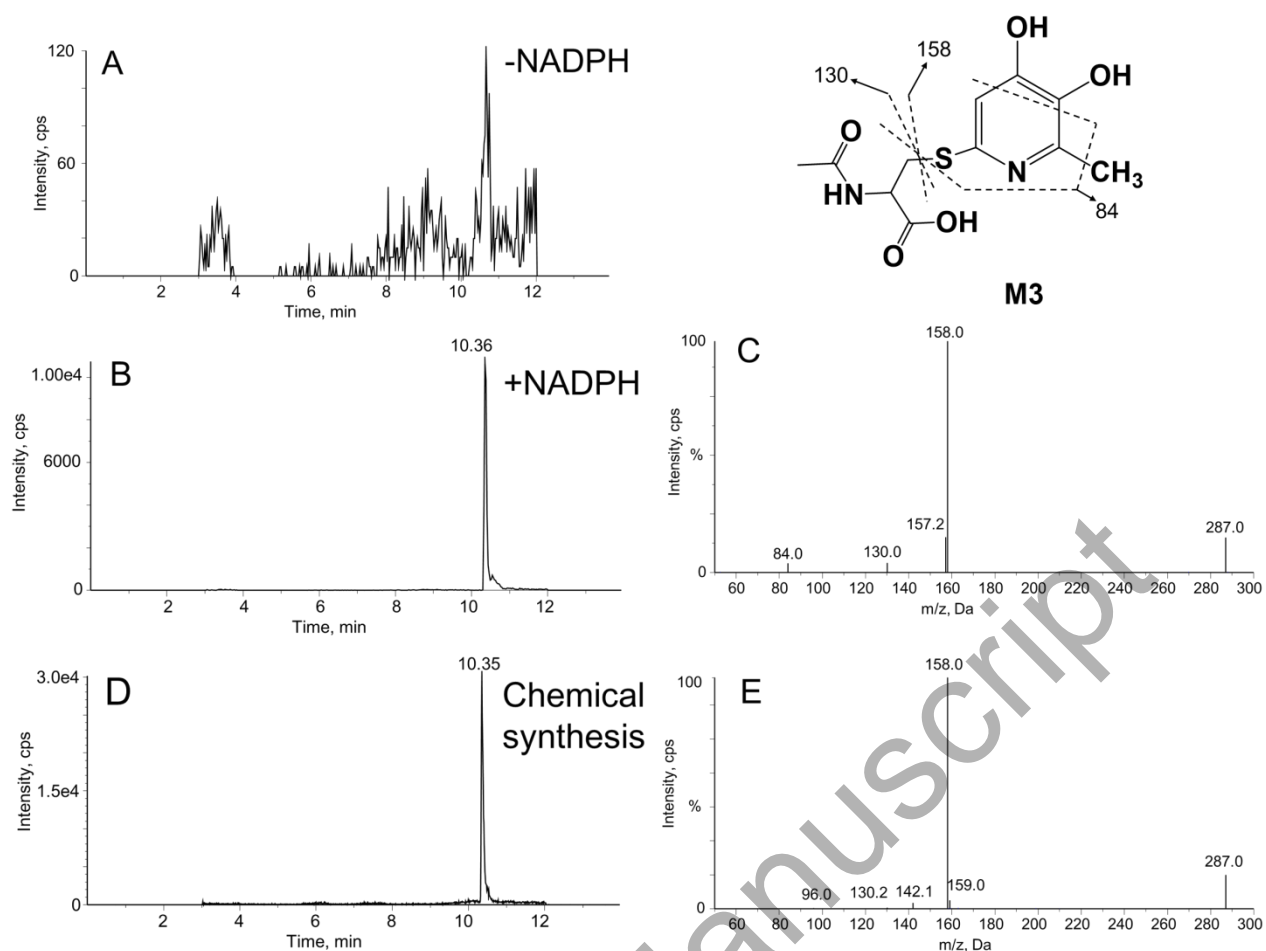
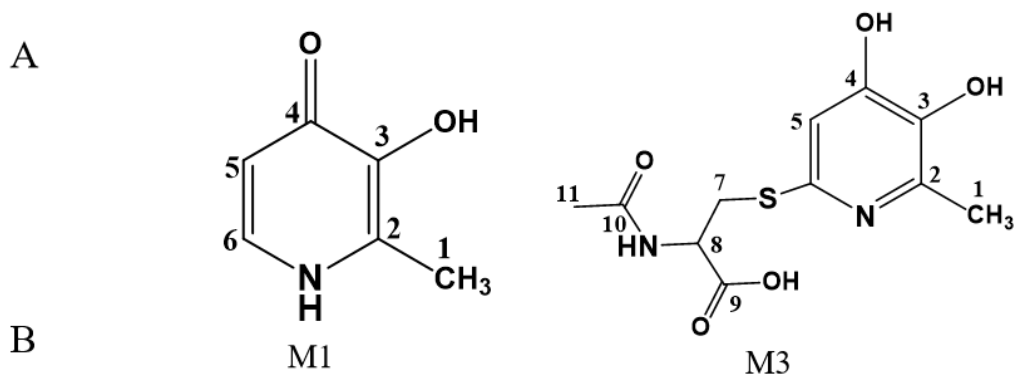


Figure 3. Characterization of M3. Extracted ion (m/z 287/158) chromatograms acquired from LC-MS/MS analysis of rat liver microsomal incubations containing DFP and NAC in the absence (A) or presence (B) of NADPH; C: Tandem mass spectrum of M3 generated in rat microsomal incubations; D: Extracted ion (m/z 287/158) chromatogram collected from LC/MS-MS analysis of synthetic M3; E: Tandem mass spectrum of synthetic M3.



Proton	M1	M3
H-1	2.17 (3H,s)	2.44 (3H,s)
H-5	6.09 (1H, d, $J=6.9$ Hz)	7.00 (1H,s)
H-6	7.40 (1H, d, $J=6.9$ Hz)	
H-7	-	3.60 (1H, dd, $J=14.6, 4.2$ Hz)
	-	3.36 (1H, dd, $J=14.6, 7.5$ Hz)
H-8	-	4.49 (1H, dd, $J=7.4, 4.1$ Hz)
H-11	-	1.90 (3H,s)
N-H	11.39 (1H,s)	-

Figure 4. Structures (A) and ^1H -NMR profiles (B) of M1 and M3.

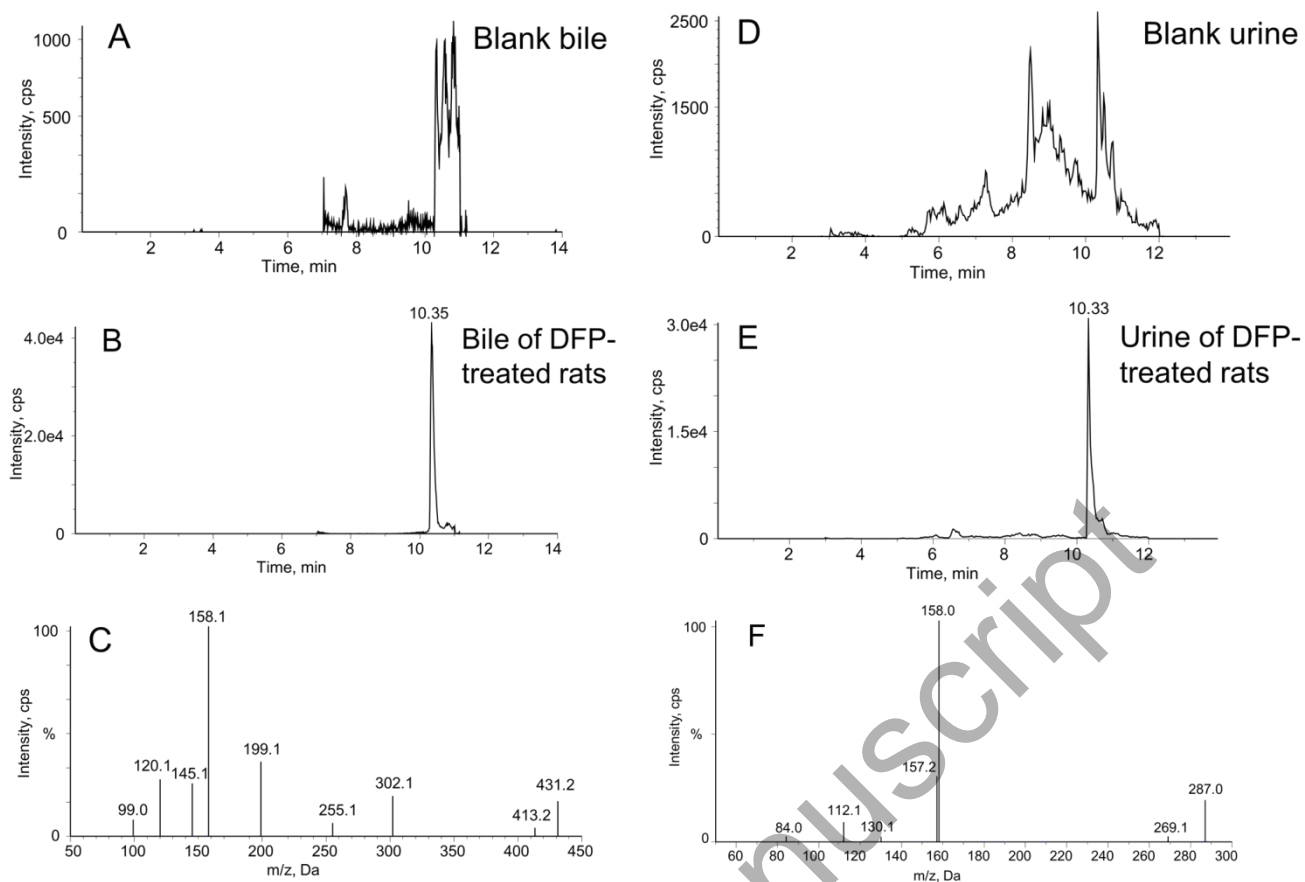


Figure 5. Characterization of biliary M2 and urinary M3. Chromatograms of extracted ion (m/z 431/158 for M2) acquired from LC-MS/MS analysis of bile harvested from rats before (A) and after (B) administration of DFP; C: Tandem mass spectrum of biliary M2 in rats treated with DFP; Chromatograms of extracted ion (m/z 287/158 for M3) obtained from LC-MS/MS analysis of urine of rats before (D) and after (E) treatment with DFP; F: Tandem mass spectrum of urinary M3 in rats administered DFP.

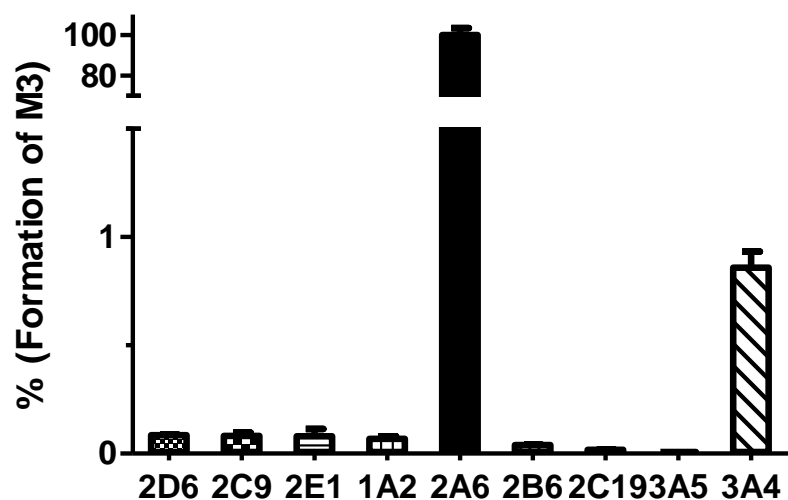


Figure 6. Role of individual human recombinant P450 enzymes in the metabolic activation of DFP. The catalytic capabilities of the enzymes were evaluated by monitoring the formation of M3 after normalization according to the relative contents of the corresponding P450 enzymes in human liver microsomes. The most abundant metabolite M3 was deemed as 100%. Data represent the mean \pm SD (n = 3).

Accepted Manuscript

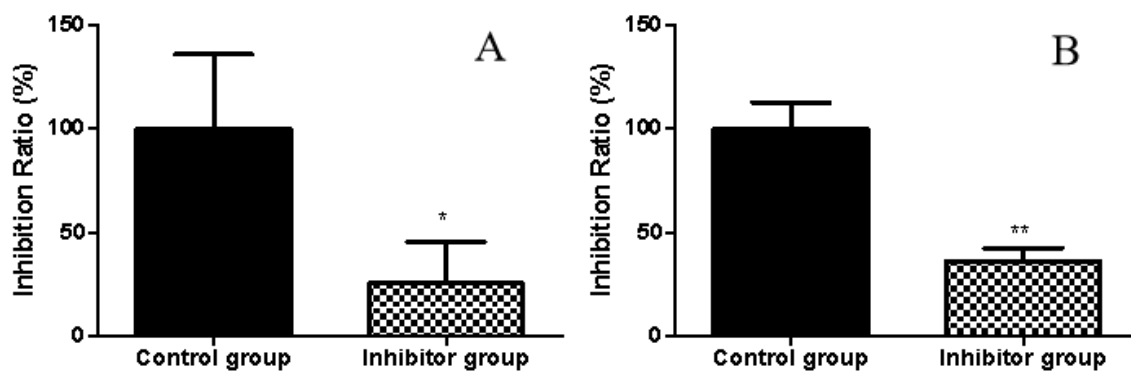
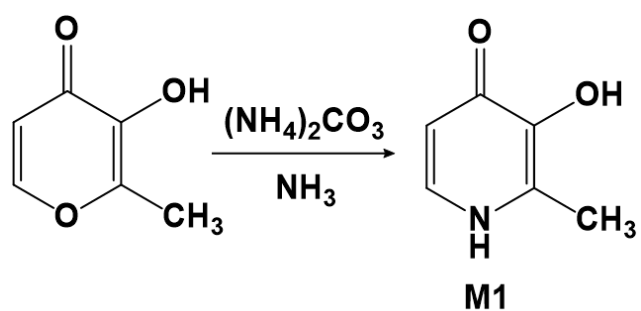


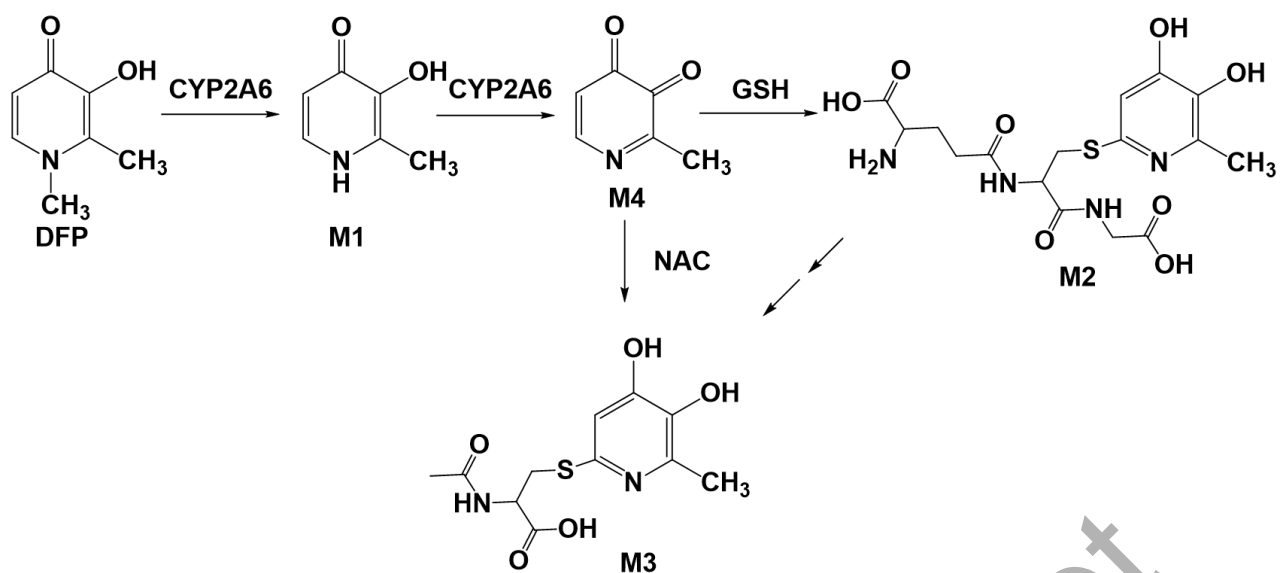
Figure 7. Inhibitory effect of methoxsalen (10 μ M) on the formation of metabolite M3 in human (A) and rat (B) liver microsomal incubations containing NAC and NADPH. The generation of M3 in control groups without methoxsalen was deemed as 100%. Data represent the mean \pm SD (n = 3). * p < 0.05; ** p < 0.01 versus their respective incubations without methoxsalen.

Accepted Manuscript



Scheme 1. Synthetic route of M1.

Accepted Manuscript



Scheme 2. Proposed metabolic pathways of DFP mediated by CYP2A6.

Accepted Manuscript